La radiologia medica
https://doi.org/10.1007/s11547-024-01771-5

CARDIAC RADIOLOGY

Imaging biomarkers in cardiac CT: moving beyond simple coronary anatomical assessment

Giulia Cundari[1] · Livia Marchitelli[1] · Giacomo Pambianchi[1] · Federica Catapano[2,3] · Luca Conia[1] · Giuseppe Stancanelli[1] · Carlo Catalano[1] · Nicola Galea[1]

Received: 1 August 2023 / Accepted: 3 January 2024

Abstract
Cardiac computed tomography angiography (CCTA) is considered the standard non-invasive tool to rule-out obstructive coronary artery disease (CAD). Moreover, several imaging biomarkers have been developed on cardiac-CT imaging to assess global CAD severity and atherosclerotic burden, including coronary calcium scoring, the segment involvement score, segment stenosis score and the Leaman-score. Myocardial perfusion imaging enables the diagnosis of myocardial ischemia and microvascular damage, and the CT-based fractional flow reserve quantification allows to evaluate non-invasively hemodynamic impact of the coronary stenosis. The texture and density of the epicardial and perivascular adipose tissue, the hypodense plaque burden, the radiomic phenotyping of coronary plaques or the fat radiomic profile are novel CT imaging features emerging as biomarkers of inflammation and plaque instability, which may implement the risk stratification strategies. The ability to perform myocardial tissue characterization by extracellular volume fraction and radiomic features appears promising in predicting arrhythmogenic risk and cardiovascular events. New imaging biomarkers are expanding the potential of cardiac CT for phenotyping the individual profile of CAD involvement and opening new frontiers for the practice of more personalized medicine.

Keywords Cardiac computed tomography angiography · Imaging biomarkers · Coronary artery disease · Myocardial tissue characterization · Fractional flow reserve · Myocardial perfusion

Abbreviations

AI	Artificial intelligence
AS	Agatston score
BMI	Body mass index
CAC	Coronary artery calcium
CAD	Coronary artery disease
CCTA	Cardiac computed tomography angiography
CFD	Computational flow dynamics
CM	Contrast media
CMR	Cardiac magnetic resonance
CT	Computed tomography
CT-LeSc	CT-adapted Leaman score
dCTP	Dynamic CT perfusion
sCTP	Static CT perfusion
CV	Cardiovascular
DECT	Dual energy computed tomography
DL	Deep learning
EAT	Epicardial adipose tissue
ECV	Extracellular volume
EMB	Endomyocardial biopsy
FAI	Fat attenuation index
FFR	Fractional flow reserve
FRP	Fat radiomic profile
HR	Hazard ratio
HU	Hounsfield units
ICA	Invasive coronary angiography
IHD	Ischemic heart disease
LGE	Late gadolinium enhancement
LIE	Late iodine enhancement
MACE	Major adverse cardiac events
MBF	Myocardial blood flow

✉ Nicola Galea
nicola.galea@uniroma1.it

[1] Department of Radiological, Oncological and Pathological Sciences, Sapienza University of Rome, Viale Regina Elena 324, 00161 Rome, Italy

[2] Department of Biomedical Sciences, Humanitas University, Via Rita Levi Montalcini, 4, Pieve Emanuele, 20090 Milano, Italy

[3] Humanitas Research Hospital IRCCS, Via Alessandro Manzoni, 56, Rozzano, 20089 Milano, Italy

Published online: 06 February 2024

MF	Myocardial fibrosis
MI	Myocardial infarction
MINOCA	Myocardial infarction with non-obstructive coronary artery
ML	Machine learning
PCAT	Pericoronary adipose tissue
PCD-CT	Photon-counting detector computed tomography
RI	Remodeling index
SIS	Segment involvement score
SSS	Segment stenosis score
VMI	Virtual monoenergetic images

Introduction

Ischemic heart disease (IHD) is the main cause of mortality in the world, responsible for around 16% of the total deaths [1]. Current prevention strategies rely on the risk stratification, acting with pharmacological treatments or lifestyle habits, and early detection of obstructive coronary artery disease (CAD). Clinical scores systems, electrocardiogram and echocardiogram demonstrated low sensitivity and specificity for the early diagnosis of CAD and prediction of major cardiovascular events (MACE) risk [2, 3]. In the last decades, cardiac computed tomography angiography (CCTA) has gained a preeminent role in the evaluation of symptomatic patients with suspected CAD, thanks to its high diagnostic accuracy and high negative predictive value. According to recent guidelines, CCTA can be considered the exam of choice to rule out obstructive CAD in patients with chronic cardiac symptoms and low clinical pre-test likelihood of disease [4–6], and in patients with acute chest pain with low-to-intermediate pre-test probability [7, 8]. However, the pure anatomical assessment of coronary arteries obtained with CCTA, does not provide functional information on lesion-specific ischemia. Recent developments in hardware and software technology, particularly with the introduction of artificial intelligence (AI) tools, are improving image quality of CCTA, increasing the detectable features of CAD (i.e., evaluation and quantification of coronary stenosis, plaque characterization, assessment of myocardial ischemia) and expanding the prognostic role of CCTA with machine-learning (ML) algorithms [9, 10]. Moreover, the use of dual energy CT (DECT) and the recent introduction of photon-counting detector scanners (PCD-CT) enabled the acquisition of ultra-high resolution images, with spectral information obtained along with each CT scan (material decomposition) and the reduction of blooming or movement artifacts together with the elimination of electronic noise [11]. The introduction of sophisticated postprocessing tools gave rise to innovative imaging biomarkers, which are, by definition, "parameters that can be measured and that may influence or predict the incidence of outcome of diseases" [12]. This new quantitative approach could improve management of patients and clinical decision making, moving toward a progressively targeted and personalized medicine. This review will focus on emerging CT imaging biomarkers, which are expanding the role of cardiac CT in individual phenotyping of CAD involvement, improving assessment of coronary stenosis and risk stratification, and characterizing myocardial tissue abnormalities.

Atherosclerotic burden

Going beyond the detection of coronary stenosis, an increasing role of CCTA is represented by the assessment of atherosclerotic burden (even in patients with non-obstructive CAD). Several CCTA scores have been developed to guide risk stratification and clinical decision-making. The Agatston score (AS) quantifies the calcium load within the coronary arteries and is globally recognized as a robust test to classify the degree of CAD e to implement cardiovascular risk stratification [13]. The coronary artery calcium (CAC) scoring, indeed, represents a class-IIa recommendation test in patients with a borderline/intermediate risk, helping in management and therapeutic tailoring [14]. CAC quantification is performed using prospective ECG-gated unenhanced CT scan [15]. The standard image analysis is based on the segmentation of any structure with density $\geq$ 130 Hounsfield Units (HU) and having an area $\geq$ of 1 mm^2 along coronary walls, as calcified focus plaque. In each segmented calcified plaque, a density score of 1–4 is assigned to each focus based on peak density (130–199 HU, 200–299 HU, 300–399 HU and $\geq$ 400 HU, respectively). The total AS is the result of the sum the scores of every coronary artery calcified focus [16] (Fig. 1).

CAC may also be measured in terms of Volume and Mass score, which measures the absolute real volume and mass of coronary calcium [15, 17, 18]. CAC quantification was found to be an excellent index of atherosclerotic plaque burden [19], showing an association between coronary calcification area, plaque volume and extent of atherosclerosis in vivo [20, 21].

Some AS cut-offs (0 = very low, 1–100 = low, 101–400 = intermediate, > 400 = high, > 1000 very high) were also proposed to differentiate in risk categories, with 10-years event rate of 22.5–28.6% and 37% in high and very high category, respectively [22]. In a recent metanalysis focusing on the role of CAC score in patients with stable or acute chest pain, the absence of CAC was associated with a very low prevalence of obstructive CAD and low risk of MACE. These results suggest the CAC score may play a role in identifying patients with stable and acute chest pain who can safely avoid additional downstream testing [23].

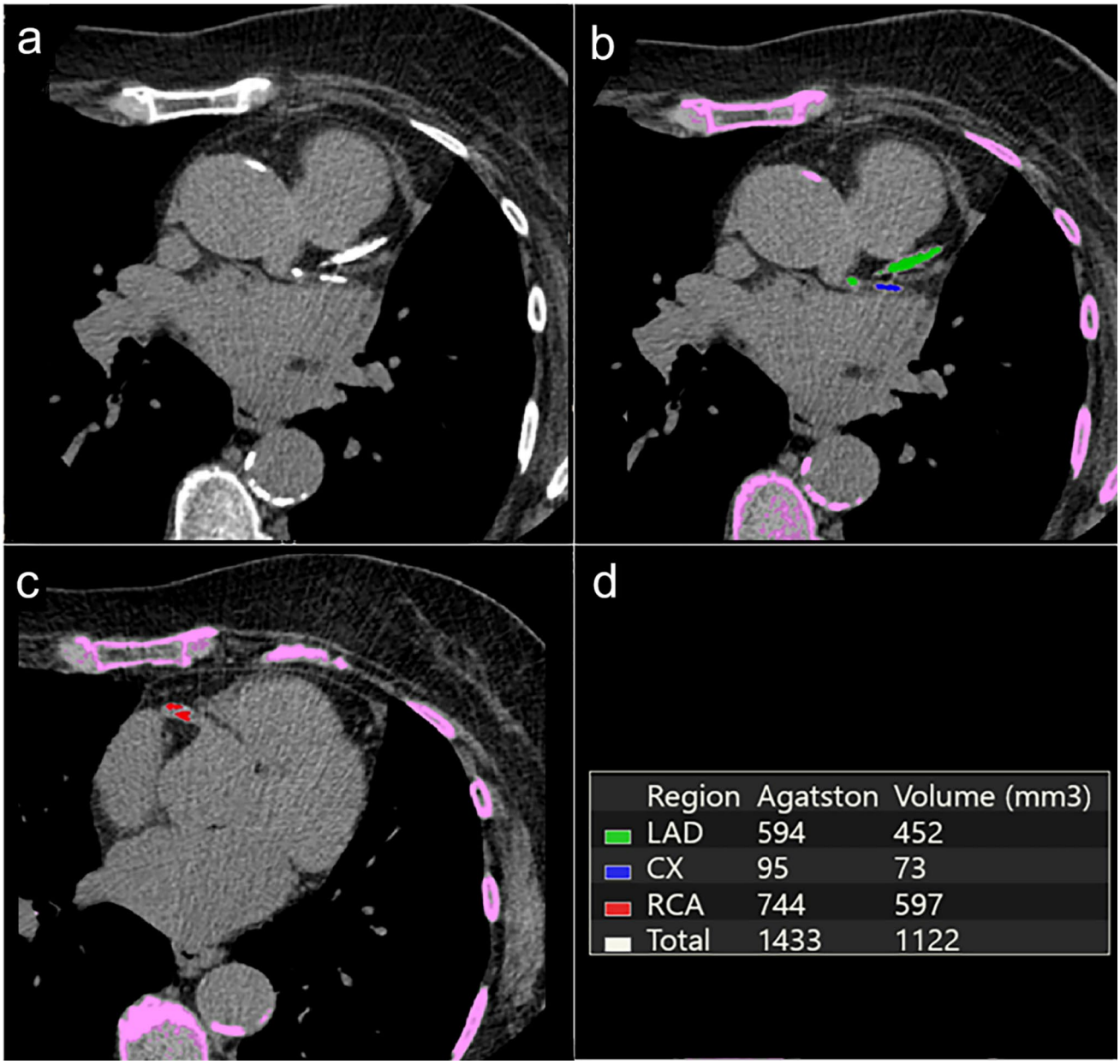

Fig. 1 Coronary Calcium Scoring. Non-enhanced CT image showing coronary calcifications on proximal LAD and CX (**a**) followed by color-coded trans-axial images that highlights moderate calcifications on proximal LAD, CX (**b**) and RCA (**c**). Agatston Score is calculated to quantify the extent of coronary calcium (**d**). CT, computed tomography; LAD, Left Anterior Descending artery, CX, Circumflex Artery; RCA, Right Coronary Artery

The accuracy of CAC quantification and classification has gradually improved over the years, in particular the CAC based on spectral data acquired with DECT [24] and new PCD-CT system allows for more accurate CAC volume estimation [25]. Both DECT and PCD-CT enable the quantification of CAC score on virtual non-contrast images (VNC), with a good agreement in assessing CAC risk categories compared to true non-contrast images [24, 26] and with a substantial increase in spatial resolution in PCD-CT. These techniques also decrease the radiation dose by eliminating the requirement for native scans typically used in standard CAC assessment.

Atherosclerotic burden may be also assessed on CCTA images. Segment Involvement Scoring (SIS) is a simple and reliable semiquantitative tool that quantifies CAD burden on CCTA (regardless of the stenosis degree), with a score ranging from 0 to 16, indicating the total number of coronary

segments affected by atherosclerotic plaques, irrespective to the stenosis degree caused [27, 28]

SIS considers also the non-calcified plaques, which may not be detected by CAC scoring scan, implementing the prognostic stratification also at early stages of CAD [28]. Based on the number of segments with disease, extent of CAD may be classified as non-extensive (≤4 segments) or extensive (>4 segments). Bittencourt et al. [29] demonstrated that among patients with nonobstructive CAD (stenosis <50%), those with extensive plaque experienced a higher rate of cardiovascular death or myocardial infarction (hazard ratio—HR, 3.1, 95% confidence interval, 1.5–6.4), than those who have non-extensive disease (HR: 1.2, 95% CI 0.7–2.4) [29]. SIS can also be combined with patients' age, in the "%SIS/age score", which adjusts SIS to the number of evaluable segments and normalizes it to patient age, with an incremental prognostic value for MACE over traditional risk factors, Agatston score and conventional CAD assessment [27]. A further evolution of the CAD categorization system was the segment stenosis score (SSS), which is generated by the sum of the scores assigned for each coronary segment, based on the degree of the vessel lumen stenosis from 0 (absence of plaques) to 3 (severe stenosis), resulting in a total score ranging from 0 to 48. The SSS showed to be an independent predictor of all-cause mortality despite the patient's age [30] (Fig. 2).

Coronary artery disease-reporting and data system (CAD-RADS) [31] aims to improve the accuracy of diagnosing and managing CAD patients. The updated 2022 CAD-RADS 2.0 classification [32] includes new elements such as plaque burden and ischemia evaluation, enabling the integration of CT-FFR or myocardial CT perfusion (CTP) data; moreover it introduces modifiers like coronary stents, high-risk plaque features, ischemia test results, and the "P" designation to classify plaque severity, based on CAC, SIS, and Visual scoring for plaque categorization [32]. Using a scale from 0 to 5, it grades coronary artery stenosis observed in CCTA images. Further investigation or hospital admission is required only for CAD-RADS categories 3, 4, and 5, whereas Invasive coronary angiography (ICA) is suggested for CAD-RADS 4 and 5 due to a likely/very likely assessment of obstructive coronary artery disease.

CT-adapted Leaman score (CT-LeSc), is based on three sets of weighting factors using a 18-segment coronary model: localization of plaques, accounting for the coronary dominance; the type of plaque, with a multiplication factor of 1 for calcified plaques and of 1.5 for noncalcified and mixed plaque; the degree of stenosis, with a multiplication factor of 0.615 for nonobstructive (<50% stenosis) and of 1 for obstructive (≥50% stenosis) lesions. The final score is calculated as the sum of the partial CT-LeSc of all evaluable coronary segments [33]. CT-LeSc showed a significant association with some traditional demographic and clinical risk factors as well as scores for pretest CAD probability and cardiovascular risk [33, 34]

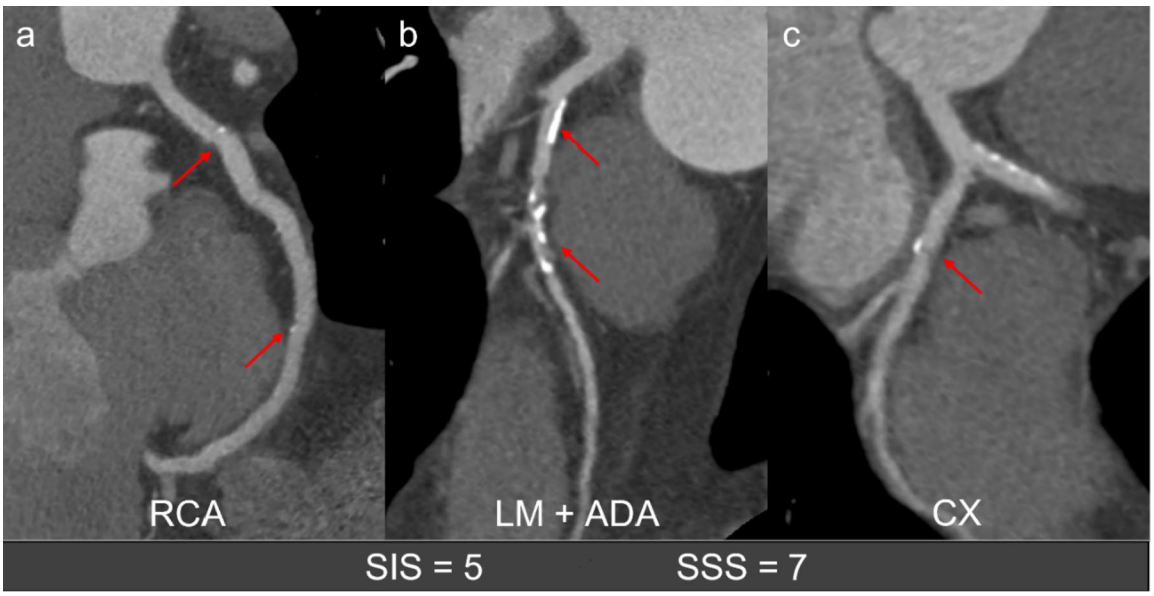

Fig. 2 Segment Involvement Score (SIS) and Segment Stenosis Score (SSS). Curved multiplanar reformatted images show a total score of 5 for SIS and a total score of 7 for SSS. Minimal stenosis both on proximal and mid RCA (1 point each, for SIS and SSS; **a** mild stenosis on proximal LAD (1 point for SIS and SSS; **b** severe stenosis on mid LAD (1 point for SIS and 3 points for SSS; **b** and mild stenosis on proximal CX (1 point for SIS and SSS; **c**. CX, Circumflex Artery; LAD, Left Anterior Descending artery; LM, Left Main; RCA, Right Coronary Artery

and demonstrated to be an independent long-term predictor of MACEs. Patients with nonobstructive CAD with a significant atherosclerotic load (CT-LeSc > 5) exhibited event-free survival compared to patients with obstructive CAD.

The Leiden CCTA risk score is a comprehensive semi-quantitative evaluation of the coronary segments, that uses different weight factors, such as the plaque location (0–6 points), the severity of the stenosis (1–1.4 points) and the composition (1–1.3 points) of coronary plaques; the score is the result of addition of each individual segment scores, which are obtained by the multiplication of these three factors [35]. It demonstrated to be able to predict major adverse cardiac events (MACEs) in both diabetic and non-diabetic patients, with suspected CAD [36].

Major limitation to the broad routine use of the quantitative or semiquantitative assessment of coronary atherosclerotic burden is the long-time image analysis and scoring calculation. AI algorithms appear promising in speeding up this process, warranting greater reproducibility and fast labeling of these data. ML and deep learning (DL) based techniques are improving image segmentation, quantification of plaques extent, stenosis assessment, identification of culprit coronary lesions and calculation of composite scores. The identification of the coronary artery stenosis severity is the most fundamental application of ML analysis (i.e., it can automatically identify coronary obstructive lesions, or classify minor coronary plaques) [37]. In this regard, Sandstedt et al. compared AI-based automatic CAC score evaluation on non-contrast CT images to semiautomatic software in 315 patients, finding an excellent correlation and agreement for three CAC scores (AS, volume score and mass score) and the number of calcified lesions ($p = 0.935$, 0.932, 0.934) [38].

High-risk coronary plaque features

CCTA may characterize the coronary plaque identifying high risk plaque features [39–41], which include:

- positive remodeling: defined as a remodeling index (RI) ≥ 1.1 [39, 42, 43], obtained by dividing the largest stenosis vessel cross-sectional area/diameter by the average cross-sectional area/diameter of the proximal and distal reference segments [44];
- intraplaque low attenuation regions: defined as mean attenuation < 30 HU in at least three regions of interest within the plaque [44] (Fig. 3);
- spotty calcifications: calcifications with more than 130 HU and a diameter < 3 mm encircled by non-calcified components [45, 46];
- napkin-ring sign: a low-attenuation core surrounded by annular high-attenuation plaque tissue [47].

Although CAD severity proved to be associated with the incidence of CV death and/or myocardial infarction (MI) [48], the PROMISE trial demonstrated that more than a half of MACE occurs in patient without coronary obstruction, suggesting that other factors must be taken into account [49]. Recent studies found an increased risk of MACE when high-risk plaques were detected on CCTA [39, 50, 51], regardless of CV risk factors and significant CAD, both for patients with stable angina and for patients admitted to the emergency department [40, 52]. Moreover, the detection of high-risk plaques can be useful in identifying significant lesions, as shown in the study from von Knebel Doeberitz et al. [53]: they found that lesion length, non-calcified plaque volume, RI, and "napkin-ring sign" were significant predictors for lesion-specific ischemia, as assessed by invasive fractional flow reserve (FFR).

Nevertheless, manual plaque quantification is time-consuming; consequently, semi-automatic plaque assessment using dedicated software has been recently introduced [54]. Semi-automated tools showed a high reproducibility (in both intra- and inter-observer comparisons) for CCTA geometrical measurements (such as lumen and vessel area and plaque burden) and a higher variability for compositional measurement (plaque attenuation and % of low attenuation plaques), ranging from 4 to 12% for inter-observer variability and 2 to 6% for intra-observer variability.

The radiomic analysis of atherosclerotic plaque may further improve CCTA diagnostic accuracy, given the ability to extrapolate quantitative features of high-risk plaques and stratify plaque risk, with low inter-observer variability. Kolossváry et al. found that 20.6% of radiomic features were significantly different between plaques with and without "napkin-ring sign" and exhibit excellent discriminatory power [55]. When compared with positron emission tomography, intravascular ultrasound and Optical Coherence Tomography plaque assessment, radiomics features on CCTA images showed good-to-excellent diagnostic accuracy in identify vulnerable plaque, surpassing conventional parameters [56].

Fractional flow reserve

Although high negative predictive value of CCTA in ruling out obstructive CAD [57], the PROMISE trial demonstrated some limitations of CT when used as initial diagnostic strategy, such as the consequent higher rate of ICA not translating into improved clinical outcomes and higher healthcare costs [58].

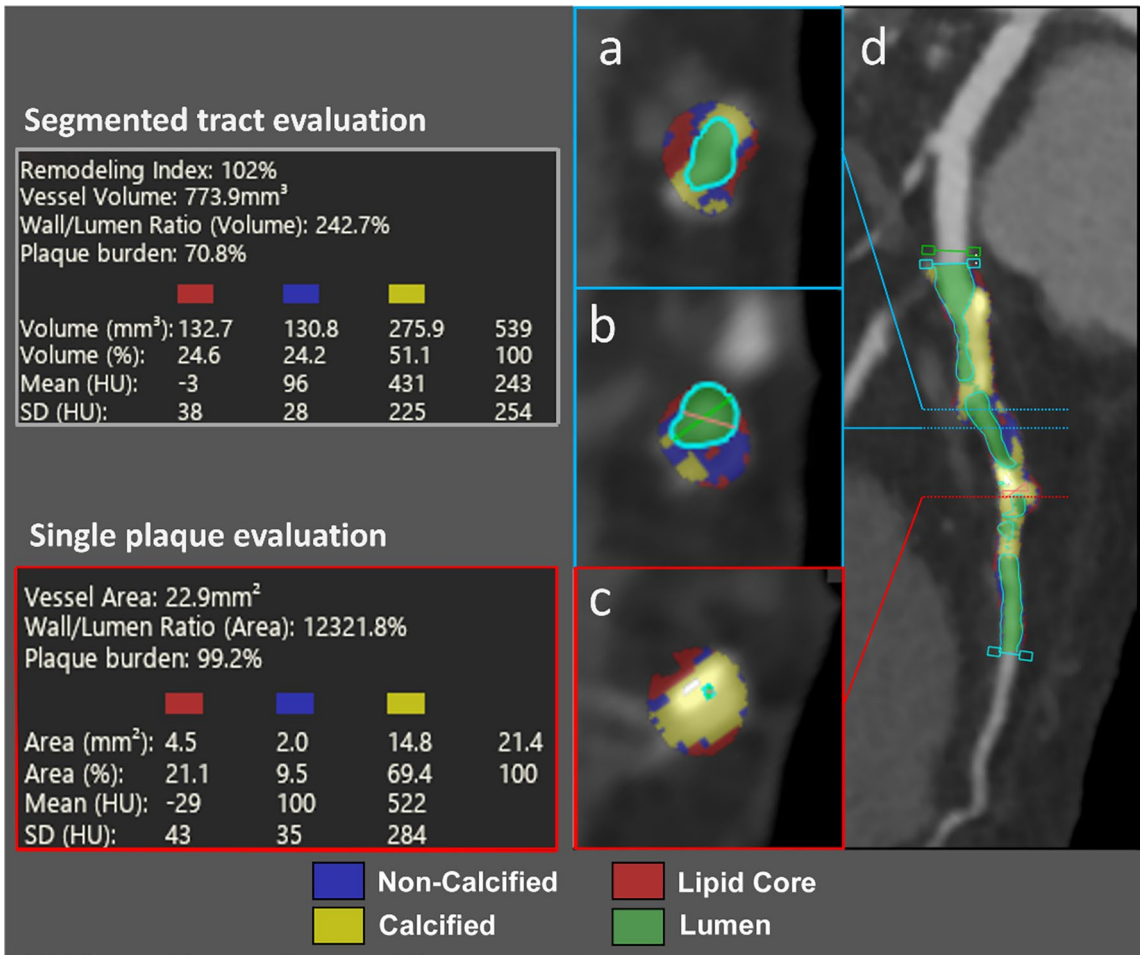

Fig. 3 Curved multiplanar reformatted image of LAD (**d**) shows multiple mixed plaques (**a**–**c**) involving proximal and mid segments. The specific components of the plaques (non-calcified, calcified and lipid core) are analyzed and quantified automatically with a dedicated software, according to their density (on the left). LAD, Left Anterior Descending artery

To improve the ability of CCTA in the identification of flow-limiting coronary stenosis, the calculation of FFR with CT (FFR-CT) is emerging as a robust and valuable tool. The most common method for the calculation of FFR-CT is based on computational fluid dynamics (CFD), a mathematical three-dimensional modeling technique which simulates intra-coronary flow, pressure, and resistance by using semi-automatic contouring and segmentation on CCTA images [59].

The generated FFR-CT values, based on patient-specific inflow and outflow hemodynamic conditions, are able to predict pressure changes along the course of the vessel. A FFR-CT value greater than 0.8 is normal, values between 0.76 and 0.8 are borderline, and values lower than or equal to 0.75 are abnormal and suggestive for significant stenosis [60] (Fig. 4).

Alongside with CFD techniques, several ML and DL-based methods for FFR-CT have been recently developed [61–64]. The retrospective multicenter MACHINE registry, comparing ML-based and CFD-based FFR-CT, showed no significant differences in the diagnostic performance of ML-approach compared to CFD algorithm [65]. ML and DL-based approaches have the advantage of not requiring transfer of imaging data into the cloud, which increases time consumption. For on-site measurement, the CT-FFR value can be provided to the physician within a day, facilitating prompt decision-making in subsequent steps [66].

In terms of diagnostic accuracy, several trials proved that FFR-CT is a valuable alternative to invasive FFR. In their prospective multicenter study, Bon-Kwon Koo et al. [67] enrolled 103 patients with stable angina who underwent both CCTA with FFR-CT and invasive FFR, demonstrating a good concordance on a per-vessel level (Spearman's rank correlation coefficient of 0.717 and a Pearson's correlation coefficient of 0.678) and no systematic differences at the per-patient level. FFR-CT showed an accuracy of 84% compared to 58.5% of CCTA alone, on a per-vessel analysis; sensitivity and specificity were 87.9% and 83% respectively.

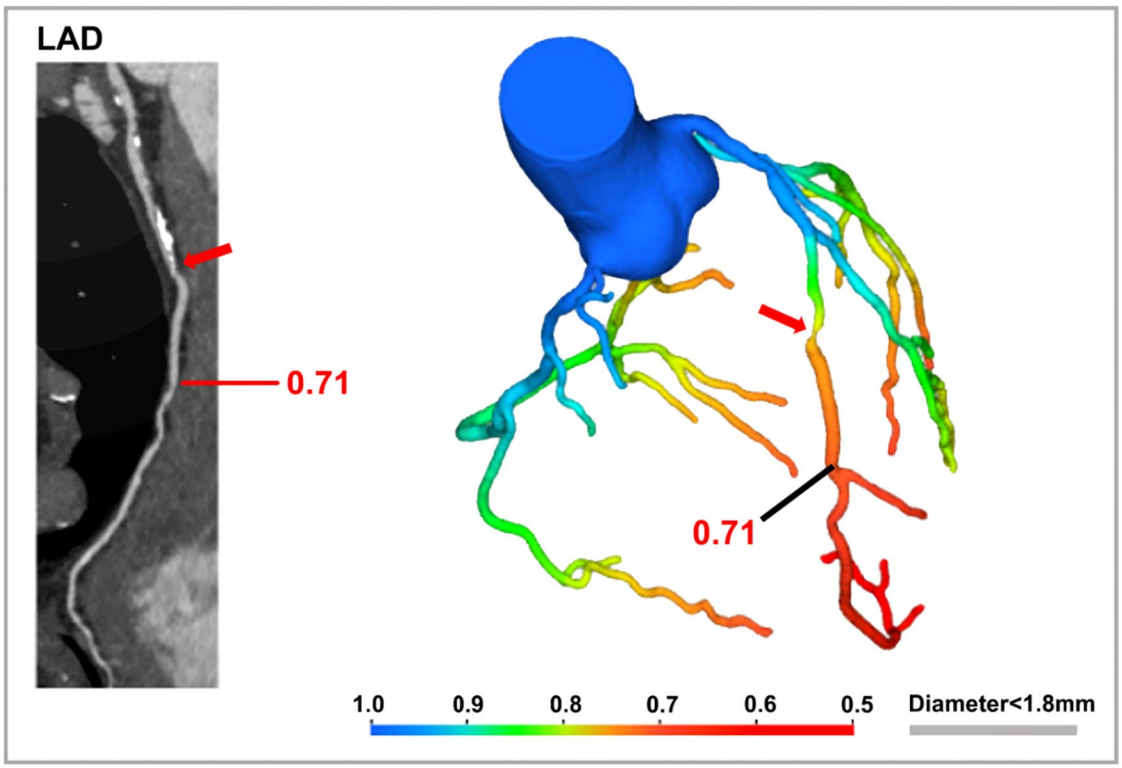

Fig. 4. 51 years-old man with high cardiovascular risk profile, performing CCTA for recurrent atypical chest pain. Curved planar reformatted images of LAD show a moderate stenosis in middle segment (red arrow). FFR-CT analysis (DeepVessel Image) reveals a significant flow reduction (FFR = 0.71) after the stenosis (red arrow). CCTA, cardiac computed tomography angiography; FFR-CT, fractional flow reserve—computed tomography; LAD, left anterior descending artery

The PLATFORM trial [68, 69] demonstrated that FFR-CT guided strategy was associated with minor rate of MACE at one year compared to the standard-of-care group (6.1% vs. 7.6%, respectively). Moreover, FFR-CT led to a significant reduction in the rate of downstream ICA procedures with median costs lower versus usual care with an invasive strategy ($p < 0.001$).

Recently Fischer et al. [70] sought to explore the role of FFR-CT in the acute setting. They observed that exclusion of hemodynamically significant CAD with FFR-CT in patients with acute chest pain results in a negative predictive value of 100% for excluding MACE at 30 days. Accordingly, the "2021 AHA/ACC/ASE/CHEST/SAEM/SCCT/SCMR Guideline for the Evaluation and Diagnosis of Chest Pain" recommended FFR-CT in intermediate-risk patients with acute chest pain and coronary artery stenosis of 40–90% in a proximal or middle segment on CCTA for diagnosis of vessel-specific ischemia and to guide decision-making regarding the use of percutaneous intervention (PCI) (IIa/B-NR) [71].

While FFR-CT has demonstrated promising results, there are several factors that limit its application in clinical practice, such as the need of optimal quality of CCTA images for adequate post-processing. In some studies, investigating the accuracy of FFR-CT, the percentage of datasets rejected ranged from 11 to 13% [67, 72, 73], reaching 33% in the PROMISE study [58]. Moreover, any inaccuracies in the modeling process can lead to subsequent errors in FFR-CT values; this is particularly valid for small branch vessels which can be left out of modeling, resulting in lack of identification of their stenosis/occlusion by FFR-CT [59].

Despite the aforementioned limitations needs to be taken into account, it should be considered that the introduction of the next-generation hardware may sharply reduce the rejection rate, as demonstrated in the study from Pontone et al. [74], which mostly includes dual-source technology and wide detector scanner, who found a significantly lower rejection rate ranging from 2.9% in the ADVANCE Registry cohort to 8.6% in the clinical cohort. Additionally, they found that temporal resolution, section thickness and heart rate are independent predictors of CCTA scan rejection for FFR-CT analysis, thus suggesting that technological advanced may potentially zeroing the rejection rate by acting on these factors.

Pericoronary adipose tissue

It is known that vascular wall inflammation may trigger atherosclerotic plaque instability and risk of rupture, altering lipid accumulation and attenuation in the pericoronary adipose tissue (PCAT) [75]. When inflammatory phenomena occur in the coronary walls, the density of PCAT changes from more negative to less negative values, due to edema and inflammatory cell infiltration (Fig. 5).

Such alterations may be assessed by the perivascular fat attenuation index (FAI) [76], which describes adipocyte lipid content and size, demonstrating excellent sensitivity and specificity for detecting tissue inflammation as assessed by tissue uptake of 18F-fluorodesossyglucose at positron emission tomography [77].

The perivascular FAI is defined as the weighted average attenuation of all voxels containing adipose tissue located within a radial distance from the external vessel wall equal to the diameter of the vessel considered [78]. It can be measured around any segment of the coronary tree, but its original standardization was performed around prespecified segments of the proximal right coronary artery and left anterior descending artery.

Pericoronary FAI is a useful biomarker to detect patients with high levels of vascular inflammation and to identify vulnerable patients at risk for MACEs [79]. As stated by Oikonomu et al. [80], perivascular FAI increases the discriminatory capacity of mortality risk and contributes to the reclassification of current risk stratification models. FAI value is useful in identifying individuals at risk of acute coronary syndrome even in absence of significant coronary stenosis, so as in the identification of vulnerable plaques in patients with known CAD contributing to better clinical and therapeutic management by also providing support in primary and secondary prevention [80].

Going beyond the conventional evaluation of FAI, that only considers the average density measures, the radiomic analysis of PCAT enables the possibility to analyze the attenuation profile considering all the spatial interactions and providing measures of heterogeneity. One of the new radiomic signature of high risk PCAT is the pericoronary Fat Radiomic Profile (FRP). This considers not only the attenuation features included in FAI but also features like fibrosis and vascularity of PCAT. Whereas FAI changes dynamically in response to acute coronary inflammation, FRP captures more permanent structural changes in PCAT and provides additional risk stratification. The combination of FAI and FRP facilitates the development of a more comprehensive individualized cardiac risk profile for each patient [76]. In this regard, Lin et al. recently demonstrated that patients with acute MI show a different PCAT radiomic phenotype as compared to stable CAD patients or healthy controls. PCAT attenuation values were significantly higher in patients with acute MI (-82.3 ± 5.5 HU) as compared to patients with stable CAD (-90.6 ± 5.7 HU, $P < 0.001$) and controls with no CAD (-95.8 ± 6.2 HU, $P < 0.001$) [81].

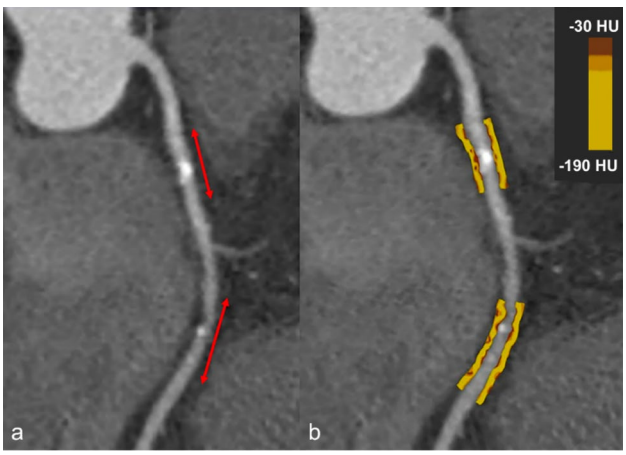

Fig. 5 Curved multiplanar reformatted (cMPR) image of LAD shows calcified plaques in proximal and mid segments (**a**). Color-coded cMPR image (**b**) highlights pericoronary adipose tissue (PCAT) attenuation gradients as a metric of vascular inflammation, indicating stable atherosclerotic plaques. LAD Left Anterior Descending artery

Myocardial perfusion imaging

Stress CT perfusion (CTP) is an emerging imaging technique which combines a pure anatomic evaluation of coronary arteries with functional data. The principle of the technique is based on quantifying the myocardial distribution of the iodinated contrast agent (Fig. 6) as it first passes through the myocardium during pharmacological stress, using vasodilator agents (e.g., Adenosine and Regadenoson) [82] and/or at rest.

Myocardial CTP imaging may involve two types of CT acquisitions: static and dynamic. Static CTP (sCTP) imaging consists in a single snapshot of the myocardial perfusion acquired at a single specific time point during the early first-pass after contrast agent injection. sCTP showed high specificity (68–98%) and sensitivity (50–96%) values, similar to other stress imaging modalities [82]. Nevertheless, sCTP accuracy may be hampered by the possibility to miss the peak of contrast attenuation, leading to false-positive or false-negative results, and limited qualitative/semiquantitative image analysis.

Dynamic CTP (dCTP) imaging may overcome some of these limitations enabling direct measurement of myocardial perfusion. It consists in serial volumetric acquisitions in free-breathing covering the whole heart during contrast injection from the first-pass arterial to the wash-out phases.

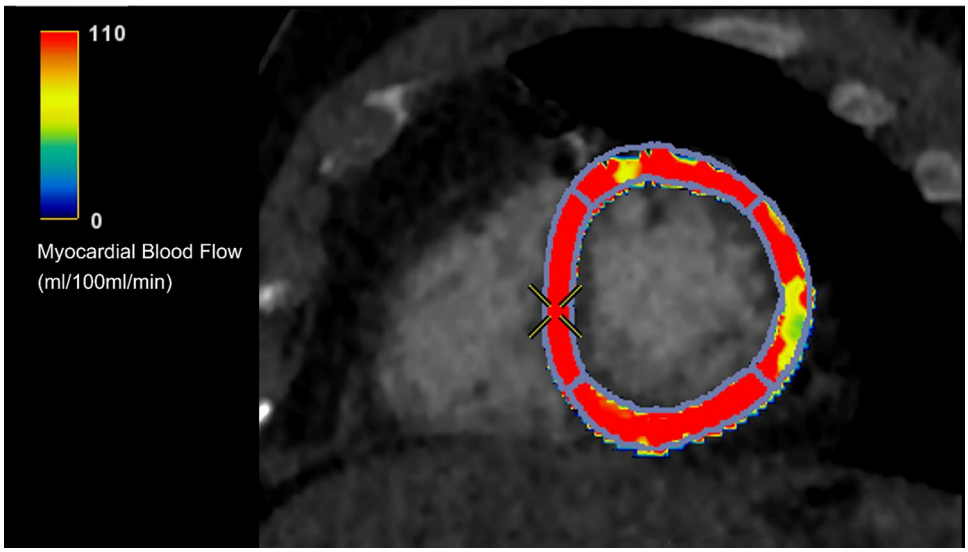

Fig. 6 Short axis color-coded parametric map of myocardial blood flow obtained during stress myocardial perfusion CT after injection of Regadenoson showing a perfusion defect in the middle lateral segment of the left ventricle

However, dCTP necessitates of at least a 256–320 slice system scanner or a dual source-CT in order to acquire multiple datasets of images; dCTP also gives a higher radiation dose than sCTP and requires longer breath holding to patients. At the image analysis, several hemodynamic parameters can be extracted, such as the myocardial blood flow (MBF), MBF ratio, and myocardial blood volume (MBV) [83].

Bamberg and colleagues, analyzing the feasibility of dCTP for the detection of significant stenosis using invasive FFR as a reference, and found a significant reduction of MBF and MBV in myocardial segments perfused by stenotic vessels; they also established a cut-off of MBF of 75 mL/100 mL/min for the differentiation between significant and non-significant coronary artery lesions (C statistic, 0.707; *P*, 0.001) [84]. Likewise, Rossi et. al computed an AUC of 0.95 (95% CI 0.92–0.98, $p < 0.001$) for MBF index, on a vessel-territory level, with sensitivity/specificity values of 90/88% in detecting significant stenosis when considering a cut-off value of 78 mL/100 mL/min [85].

dCTP showed greater and additional discriminative effectiveness compared to CCTA alone in various studies [83, 85–88]. In particular, the main diagnostic benefit in detecting significant stenosis of dCTP consists in increasing the specificity value from 61 to 81% as reported in a recent meta-analysis [89]. Moreover, in a multicenter randomized controlled trial, Lubbers et al. [90] demonstrated that a comprehensive CCTA protocol with myocardial perfusion led to fewer additional noninvasive testing and shorter diagnostic pathways.

Myocardial perfusion may also ameliorate prognostic prediction, as the summed stress score, determined by normalizing MBF using CTP, is a better predictor of MACE then coronary stenosis at CCTA, with a hazard ratio of 5.7 (95% confidence interval: 1.9–16.9; $p = 0.002$) [91]. MBF extracted from dCTP is also highly accurate in the assessment of microvascular obstruction [92], which is known to be a predictor of MACE in patients with myocardial infarction and preserved ejection fraction [93].

Finally, given that iodine is delivered to myocardial tissue by blood flow supply, recent studies suggest iodine distribution maps by DECT as a marker of myocardial perfusion [94, 95]. Introducing iodine perfusion maps increases the diagnostic accuracy of CCTA scans compared to cardiac magnetic resonance (CMR), single-photon computed tomography and ICA [96].

Late iodine enhancement

Imaging of myocardial fibrosis (MF) is based on contrast agent accumulating in myocardial tissue areas which demonstrate an expansion of extracellular matrix or in the intracellular space of necrotic myocytes [97]. Late gadolinium enhancement (LGE) imaging by CMR represents the reference standard to assess MF in vivo, but several contraindications to CMR exist together with the long image acquisition times, which limits its use. The evaluation of MF scars has also been developed with CT, based on the extracellular properties of iodine CM and the visualization of hyperenhanced areas due to iodine accumulation [98], showing a diagnostic accuracy of 88–95% as compared to CMR-LGE [99] and a diagnostic accuracy of 90%, with 53% sensitivity and 98% specificity, if compared to histological examination [100] (Fig. 7).

Several protocols exist regarding the injection of CM and the timing of late-phase acquisition: the majority of the authors report a single-bolus administration technique, so the late phase is acquired after the standard dose of CM injected for CCTA, with no further amount of CM; in other cases, a bolus-continuous protocol is performed,

Fig. 7 Late iodine enhanced (LIE) CT image reconstructed in four chamber view (**a**) and late gadolinium enhanced (LGE) image acquired on the corresponding plane during a cardiac-MR (**b**) in a patient with an acute myocardial infarction of the left circumflex artery territory. In both images is evident the contrast enhancement of the infarcted myocardium (white and black arrows) and the thrombi adherent to the apex in both ventricles (white arrowheads)

with an additional continuous infusion of CM (30–90 mL at 0.1–0.3 mL/s) after the CCTA scan. The optimal timing for the late phase scan ranges between 5 and 15 min, with the best results reported between 10 and 15 min using the bolus-continuous protocol [98].

Because of poor contrast resolution in the delayed-phase CT scan, especially for subepicardial scars, the assessment of MF can be challenging [99]. Values of diagnostic accuracy vary according to the image reconstructions algorithms that are applied, ranging from a sensitivity and specificity of 56% and 93% (with filtered back projection) to 80% and 91% (with knowledge based iterative model reconstruction), respectively [101]; and sensitivity decreases with the increasing in tube voltage kVp reconstructions, ranging from 98% at 100 kVp, to 28% at 140 kVp [102]. In this regard, the use of low tube voltages (80–100 kVp) and specific denoising reconstruction algorithms can improve contrast-to-noise ratio and reduce the radiation dose to the patients [103].

DECT and PCD-CT technology allow for spectral evaluation and virtual monoenergetic images (VMI) reconstruction at lower KeV, resulting in improved contrast-to-noise ratio for LIE evaluation [100]. Spectral CT demonstrated a sensitivity of 82% and a specificity of 99% among a population of patients with CMR-proven acute myocarditis [104]. Using iodine-density imaging, sensitivity was 97.1% and specificity 88.9% in patients with heart failure, with the highest diagnostic accuracy obtained for 40-keV VMI reconstructions (90.8%) [105]. LIE can also be used to investigate acute chest pain patients admitted to emergency department with troponin increase [106]: with this approach, patients are scanned in the angiographic phase to rule out (obstructive coronary artery disease, acute aortic syndromes and pulmonary embolism) and in the late phase for myocardial tissue characterization. Other applications include the assessment of myocardial scars as a substrate for ventricular arrhythmias prior to radiofrequency catheter ablation procedures [107].

Extracellular volume fraction

Extracellular volume fraction (ECV) assessed using T1 mapping sequences by CMR (ECV_{CMR}) has emerged as valuable surrogate marker of interstitial fibrosis, calculated by the amount of gadolinium distributed in the myocardium in the equilibrium phase [108]. ECV may be assessed also with CT (ECV_{CT}) with similar approach [109], overcoming the aforementioned contraindications related to CMR [110]. Recent studies that compared ECV_{CMR} with ECV_{CT} among patients with amyloidosis, aortic stenosis, pulmonary hypertension, or dilated cardiomyopathy achieved correlation coefficients ranging from 0.73 to 0.91 [111, 112], whereas the correlation between collagen volume fraction at histology and ECV_{CT} values in a population with severe aortic stenosis was 0.71 ($p = 0.0007$) [109].

ECV measurements can be performed with single-energy acquisitions, with DECT or PCD-CT [113] (Fig. 8).

In the former method, ECV_{CT} is derived by combining the differences in attenuation in myocardial tissue and blood pool, between the delayed scan and the non-enhanced scan.

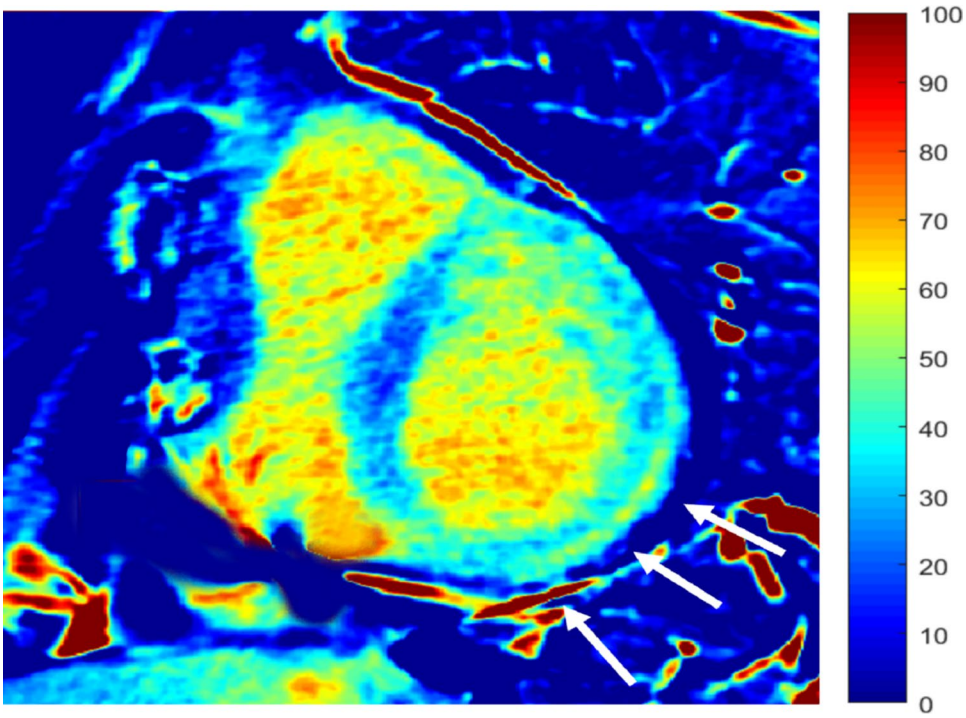

Fig. 8 CT-derived extracellular volume fraction (ECV_{CT}) map on a mid-ventricular short axis slice acquired in a 43-years-old woman with history of ventricular tachycardia and previous ICD implantation. The map shows a diffuse increase of ECV in the lateral wall (white arrows) associated to a thin subepicardial rim of focally increased ECV compatible with scarring fibrosis. The patient was diagnosed with chronic myocarditis. *ICD: implantable cardioverter device*

However, this technique can be associated with misregistration artifacts (non-matching images between baseline and late phases) and a greater radiation dose to the patients [114, 115]. With DECT or PCD-CT, ECV_{CT} is quantify by measuring the iodine concentration in myocardium and blood pool in the delayed-phase scan only, based on spectral decomposition of the obtained multi-energy datasets [110]. The acquisition time for the delayed scan phases is not still unanimously shared, ranging from 5 to 12 min [114, 116]; CM injection technique could be based on single or double boli (fixed or proportional to patient's body weight [117–119]) or with slow intravenous infusion [109, 115].

ECV_{CT} represents a promising biomarker, that could support the management of cardiac diseases associated to the development of MF, improving the prediction of MACE [120], mortality [121] or progression to heart failure [122, 123] and addressing specific therapies.

Epicardial adipose tissue

Epicardial adipose tissue (EAT) typically appears as a hypodense layer lying between the myocardial wall and the visceral pericardium, with a density ranging from − 190 to − 30 HU containing the coronary vessels and their principal branches [124–126] (Fig. 9).

In the last few decades, growing attention have been focused on EAT as a biomarker of CV risk, as an increased EAT volume has shown a strong association with CV pathologies, including CAD and ischemic heart disease [127, 128]. Specifically, Mancio et al. [125] showed that EAT volume was associated with coronary stenosis, myocardial ischemia, and MACE, irrespective from CV risk factors.

Increased EAT volume has also proven to be a strong predictor for the risk of atrial fibrillation [129], regardless of other risk factors, including left atrium diameter [130]. In patients with heart failure with preserved ejection fraction, greater EAT deposition have been associated with higher body mass index (BMI), cardiac structural changes, and proteomic markers linked to general obesity, systemic inflammation, insulin resistance, endothelial dysfunction, and dyslipidemia [131]. EAT volume quantification is feasible on both non-contrast cardiac-CT and CCTA image data sets, even though the presence of contrast media (CM) may lead to an underestimation of EAT volume [132].

Beyond the volumetric quantification, the analysis of EAT radiodensity may also serve as an imaging biomarker, as it may reflect inflammation or metabolic activity of EAT [133]. Franssens et al. [134] found a significant association between low CT attenuation of EAT and a higher amount of CAC in men with higher CV risk or overt CV pathology, regardless of EAT volume and BMI. Accordingly, serum levels of plaque inflammatory markers, coronary calcification, and MACE were all linked with lower EAT density in a study from Goeller and colleagues [135]. Finally, a rise in EAT radiodensity is also associated with Tako-Tsubo syndrome and myocardial infarction with non-obstructive coronary artery (MINOCA) [136].

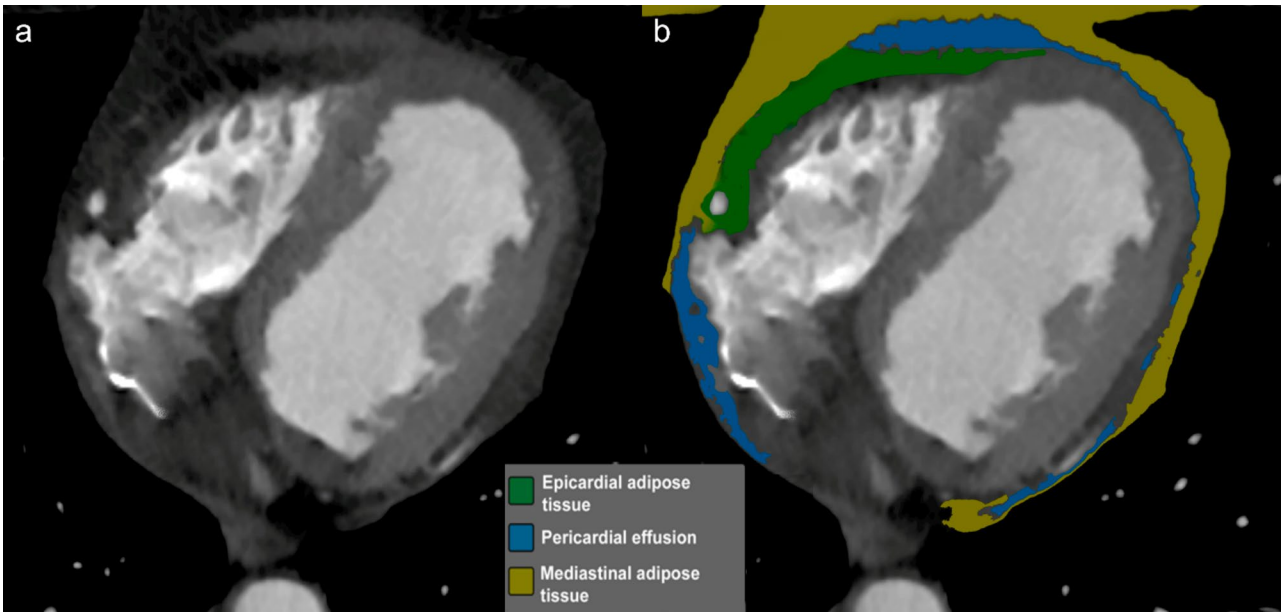

Fig. 9 Axial CT (**a**) and corresponding color-coded map (**b**) showing different pericardial (yellow) and epicardial (green) adipose tissue compartments

Besides manual quantification, which may be highly time-consuming, in the last few years methods allowing semi-automatic [135, 137, 138] and automatic segmentation [139, 140], including DL approaches [141, 142], have been investigated. Specifically, the adoption of fully automated segmentation techniques may provide the benefit of high reproducibility for EAT volumes calculation with quicker segmentation times, optimizing EAT quantification for clinical use [141].

Future perspectives

The introduction of radiomics into the medical field represents a chance to explore quantitative data through the extraction of multiple image-based features that are imperceptible to the naked eye [143]. The initial experience using radiomics analysis in cardiac CT imaging [144–149] indicate that this technique may help in identifying vulnerable plaques, improve cardiac risk stratification and open new frontiers for personalized cardiovascular medicine [150]. On the other hand, research into potential applications of AI in diagnostic imaging has gained growing interest in the last decade, and cardiac imaging was not an exception. With the rise of commercially available or open-source AI algorithms, the workflow of postprocessing analysis and interpretation of CCTA imaging datasets is changing dramatically. The optimization and speeding up of procedures guaranteed by AI tools, are expanding the role of CCTA for risk stratification as well as for patient treatment planning and management [151].

The progressive validation of new CT imaging biomarkers will expand the role of Cardiac CT in the next few years, moving beyond the simple assessment of stenosis to risk stratification and characterization of tissue alterations (Table 1). The automatic extraction of various quantitative parameters from cardiac CT imaging dataset could open a new era, where several features of vulnerability, functional parameters and markers of tissue changes will be provided, enabling deeper phenotyping of the disease and addressing to personalized therapeutic approach.

Table 1 Summary of CT imaging biomarkers

Biomarker	Acquisition Technique	Contrast administration (Phase)	Definition	Utility	Advantages	Limitations
Calcium score (Agatston Score, calcium volume and mass)	ECG-gated unenhanced scan	No	Measurement of the amount of calcium in the coronary arteries wall	Estimation of CAD burden Improvement of risk stratification for MI or other MACEs (including in asymptomatic patients)	Low radiation dose No use of contrast agents Easy post-processing	No standardized extraction of calcium scores values from CCTA images Inability to discriminate between focal and scattered calcified plaques Inability to detect non-calcified plaques
Segment Involvement Score (SIS)	ECG-gated contrast enhanced scan	Yes (arterial)	Total number of coronary segments with atherosclerotic plaque		Semi-quantitative assessment Considers both calcified and non-calcified plaques Indicator of CAD also at early stages	Time-consuming analysis Poor discrimination between patients with or without flow-limiting stenosis and/or requiring revascularization
Segment Stenosis Score (SSS)	ECG-gated contrast enhanced scan	Yes (arterial)	Summation of the extent scores of all 16 individual segments Score is calculated as: 0 = no plaque; 1 = < 50%; 2 = 50–69%; 3 = > 70%			
Leaman score	ECG-gated contrast enhanced scan	Yes (arterial)	A score based on 3 weighted factors of coronary plaques: (1) localization; (2) type of plaque; (3) degree of stenosis (< 50 ≥ % stenosis) for each segment. The total score represents the sum of partial score for each segment			
Leiden score	ECG-gated contrast enhanced scan	Yes (arterial)	A score based on: plaque location (0–6 points); the severity of the stenosis (1–1.4 points) and the composition (1–1.3 points) of coronary plaques. The total represents the addition of each individual segment scores, obtained by the multiplication of these three factors			

Table 1 (continued)

Biomarker	Acquisition Technique	Contrast administration (Phase)	Definition	Utility	Advantages	Limitations
CAD-RADS 2.0	ECG-gated contrast enhanced scan	Yes (arterial)	The score is mainly based on the stenosis of most severe degree. The updated classification includes: plaque burden; ischemia evaluation (integration of CT-FFR or CTP); modifiers like coronary stents, high-risk plaque features, ischemia test results, and plaque severity, based on CAC, SIS, and Visual scoring	It offers practical recommendation for clinical management of the patients	It combines information on the degree of stenosis, atherosclerotic burden and plaque characteristics	Simplistic scoring system Time Consuming It is particularly conditioned by the degree of the major stenosis Low reproducibility of high risk plaque features
Fractional Flow Reserve (FFR-CT)	ECG-gated contrast enhanced scan	Yes (arterial)	Computational fluid dynamic-based estimation of blood flow through vessels affected by coronary stenosis using a CT anatomical 3D model	Estimation of coronary flow Detection of flow-limiting stenosis	Valuable alternative to invasive FFR High Negative Predictive Value Improving selection of patients candidate to ICA	Limited accessibility as a result of the pay-per-service approach Single provider approved for clinical use
Pericoronary Adipose Tissue (FAI; FRP)	ECG-gated (contrast enhanced or unenhanced) scan	Not necessary	FAI: average weighted attenuation of adipose tissue-containing voxels surrounding the coronary FRP: radiomic mapping of the pericoronary space based on various form, attenuation, and texture-related characteristics	Improvement of risk stratification for MI or other MACEs Information on metabolic activity of PCAT (fat browning)	Useful in assessment of vulnerable plaque not associated with significant stenosis Possibility of application of radiomic tools	Time consuming analysis Few available dedicated software Influence of acute coronary inflammation on FAI
Static myocardial perfusion	ECG-gated contrast enhanced scan	Yes (arterial)	Myocardial iodine distribution acquired at a single specific time point during the early arterial phase	Detection of coronary artery lesion-specific ischemia	Combined CT perfusion and CCTA in a single image dataset Short exam duration (compared to other cardiac functional tests) Rapid analysis Lower radiation dose	Qualitative/semiquantitative analysis (dedicated software) Need for wide coverage CT scanner High-dependance on acquisition time Non-standardized evaluation of the iodine distribution maps Use of stressor agents

Table 1 (continued)

Biomarker	Acquisition Technique	Contrast administration (Phase)	Definition	Utility	Advantages	Limitations
Dynamic myocardial perfusion (MBF and MBV)	Serial ECG-gated contrast enhanced scans	Yes (from arterial to washout)	Myocardial iodine distribution acquired over consecutive volumetric scans during passage of contrast agent	Detection of coronary artery lesion-specific ischemia	Direct measurement of myocardial perfusion throughout quantitative analysis Less influence of acquisition time Short exam duration (compared to other cardiac functional tests)	Increased radiation and contrast dose Longer breath-hold Spatial misalignment resulting from table movements Need for wide coverage CT scanner Time-consuming analysis (dedicated software) Use of stressor agents
Late Iodine Enhancement	ECG-gated contrast enhanced scan	Yes (late, 5–12 min after injection)	Myocardial areas with a focal increase of attenuation compared with remote myocardium	Detection of myocardial fibrosis	Feasible also in patients with CMR contraindications (implantable devices, claustrophobia) Applicable in setting of emergency (e.g., acute chest pain patients with troponin increase) Shorter exam duration as compared to CMR	Lower contrast to noise ratio than CMR Increased radiation exposure as compared to CCTA alone
Extracellular Volume Fraction (ECV_{CT})	ECG-gated unenhanced + contrast enhanced scan	Yes (late, 5–12 min after injection)	Extracellular volume fraction mapping using iodine distribution during equilibrium phase	Quantification of extracellular matrix expansion	Feasible also in patients with CMR contraindications (implantable devices, claustrophobia) Shorter exam duration as compared to CMR Only late phase scan if spectral imaging is used	Preferable latest generation scanner for dose control and imaging optimization Misregistration artifacts Increased radiation exposure as compared to CCTA alone Need for dedicated software
Epicardial Fat Volume/ Density	ECG-gated (contrast enhanced or unenhanced) scan	Not necessary	Quantification of epicardial adipose tissue volume and density	Improvement of risk stratification for MI or other MACEs Information on metabolic activity of EAT (fat browning)	Providing information on metabolic and inflammatory status	Time consuming analysis Few available dedicated software

CMR, cardiac magnetic resonance; CCTA, coronary computed tomography angiography; CT, computed tomography; FFR-CT, CT-derived fractional flow reserve; CV, cardiovascular; FAI, Fat Attenuation Index; FRP, Fat Radiomic Profile; ICA, invasive coronary angiography; MACE, major adverse cardiac event; MBF, Myocardial Blood Flow; MBV, myocardial blood volume; PCAT, pericoronary adipose tissue; ECV_{CT}, CT Extracellular Volume

Conclusion

The role of CCTA has progressively grown from the mere detection of obstructive CAD, by the anatomical assessment of coronary stenosis, to an examination that enables the extrapolation of multiple parameters, useful for a more accurate evaluation of cardiovascular risk and the hemodynamic effect of stenosis. In addition, new applications of CT (e.g.,, LIE, ECV_{CT}) are expanding its domain to the characterization of myocardial damage [152] and improving prognostic stratification, moving toward an increasingly comprehensive examination.

Funding Open access funding provided by Università degli Studi di Roma La Sapienza within the CRUI-CARE Agreement. The authors declare that no funds, grants, or other support were received during the preparation of this manuscript. The authors have no relevant financial or non-financial interests to disclose.

Declarations

Conflict of interest The authors have not disclosed any Conflict of interest.

Ethical statement This article does not contain any studies with human participants or animals performed by any of the authors.

References

1. The top 10 causes of death. www.who.int/news-room/fact-sheets/detail. Accessed 26 Jul 2023
2. Pugliese L, Ricci F, Sica G et al (2023) Non-contrast and contrast-enhanced cardiac computed tomography imaging in the diagnostic and prognostic evaluation of coronary artery disease. Diagnostics 13:2074. https://doi.org/10.3390/diagnostics13122074
3. Catapano F, Galea N, Pambianchi G et al (2023) Effectiveness of clinical scores in predicting coronary artery disease in familial hypercholesterolemia: a coronary computed tomography angiography study. Radiol Med 128:445–455. https://doi.org/10.1007/s11547-023-01610-z
4. Knuuti J, Wijns W, Saraste A et al (2020) 2019 ESC Guidelines for the diagnosis and management of chronic coronary syndromes. Eur Heart J 41:407–477. https://doi.org/10.1093/eurheartj/ehz425
5. Kelion AD, Nicol ED (2018) The rationale for the primacy of coronary CT angiography in the National Institute for health and care excellence (NICE) guideline (CG95) for the investigation of chest pain of recent onset. J Cardiovasc Comput Tomogr 12:516–522. https://doi.org/10.1016/j.jcct.2018.09.001
6. Esposito A, Gallone G, Palmisano A et al (2020) The current landscape of imaging recommendations in cardiovascular clinical guidelines: toward an imaging-guided precision medicine. Radiol Medica 125:1013–1023. https://doi.org/10.1007/s11547-020-01286-9
7. Collet J-P, Thiele H, Barbato E et al (2021) 2020 ESC Guidelines for the management of acute coronary syndromes in patients presenting without persistent ST-segment elevation. Eur Heart J 42:1289–1367. https://doi.org/10.1093/eurheartj/ehaa575
8. Galea N, Bellu R, Catapano F et al (2022) Coronary computed tomography angiography in acute chest pain: a sustainable model with remote support. Eur J Radiol 151:110277. https://doi.org/10.1016/j.ejrad.2022.110277
9. Muscogiuri G, Van Assen M, Tesche C et al (2020) Artificial intelligence in coronary computed tomography angiography: from anatomy to prognosis. Biomed Res Int 2020:1–10. https://doi.org/10.1155/2020/6649410
10. Lanzafame LRM, Bucolo GM, Muscogiuri G et al (2023) Artificial intelligence in cardiovascular CT and MR imaging. Life 13:507. https://doi.org/10.3390/life13020507
11. Alizadeh LS, Vogl TJ, Waldeck SS et al (2023) Dual-energy CT in cardiothoracic imaging: current developments. Diagnostics 13:2116. https://doi.org/10.3390/diagnostics13122116
12. Strimbu K, Tavel JA (2010) What are biomarkers? Curr Opin HIV AIDS 5:463–466. https://doi.org/10.1097/COH.0b013e32833ed177
13. Kapoor K, Cainzos-Achirica M, Nasir K (2020) The evolving role of coronary artery calcium in preventive cardiology 30 years after the Agatston score. Curr Opin Cardiol 35:500–507. https://doi.org/10.1097/HCO.0000000000000771
14. Arnett DK, Blumenthal RS, Albert MA et al (2019) 2019 ACC/AHA guideline on the primary prevention of cardiovascular disease: a report of the American college of cardiology/American heart association task force on clinical practice guidelines. Circulation. https://doi.org/10.1161/CIR.0000000000000678
15. Greenland P, Blaha MJ, Budoff MJ et al (2018) Coronary calcium score and cardiovascular risk. J Am Coll Cardiol 72:434–447. https://doi.org/10.1016/j.jacc.2018.05.027
16. Agatston AS, Janowitz WR, Hildner FJ et al (1990) Quantification of coronary artery calcium using ultrafast computed tomography. J Am Coll Cardiol 15:827–832. https://doi.org/10.1016/0735-1097(90)90282-T
17. Hong C, Becker CR, Schoepf UJ et al (2002) Coronary artery calcium: absolute quantification in nonenhanced and contrast-enhanced multi-detector row CT studies. Radiology 223:474–480. https://doi.org/10.1148/radiol.2232010919
18. Rumberger JA, Kaufman L (2003) A rosetta stone for coronary calcium risk stratification: agatston, volume, and mass scores in 11,490 individuals. Am J Roentgenol 181:743–748. https://doi.org/10.2214/ajr.181.3.1810743
19. Rumberger JA, Simons DB, Fitzpatrick LA et al (1995) Coronary artery calcium area by electron-beam computed tomography and coronary atherosclerotic plaque area. Circulation 92:2157–2162. https://doi.org/10.1161/01.CIR.92.8.2157
20. Baumgart D, Schmermund A, Goerge G et al (1997) Comparison of electron beam computed tomography with intracoronary ultrasound and coronary angiography for detection of coronary

atherosclerosis. J Am Coll Cardiol 30:57–64. https://doi.org/10.1016/S0735-1097(97)00147-2
21. Sangiorgi G, Rumberger JA, Severson A et al (1998) Arterial calcification and not lumen stenosis is highly correlated with atherosclerotic plaque burden in humans: a histologic study of 723 coronary artery segments using nondecalcifying methodology. J Am Coll Cardiol 31:126–133. https://doi.org/10.1016/S0735-1097(97)00443-9
22. Hecht HS (2015) Coronary artery calcium scanning. JACC Cardiovasc Imaging 8:579–596. https://doi.org/10.1016/j.jcmg.2015.02.006
23. Agha AM, Pacor J, Grandhi GR et al (2022) The prognostic value of CAC zero among individuals presenting with chest pain. JACC Cardiovasc Imaging 15:1745–1757. https://doi.org/10.1016/j.jcmg.2022.03.031
24. Gassert FG, Schacky CE, Müller-Leisse C et al (2021) Calcium scoring using virtual non-contrast images from a dual-layer spectral detector CT: comparison to true non-contrast data and evaluation of proportionality factor in a large patient collective. Eur Radiol 31:6193–6199. https://doi.org/10.1007/s00330-020-07677-w
25. van der Werf NR, Si-Mohamed S, Rodesch PA et al (2022) Coronary calcium scoring potential of large field-of-view spectral photon-counting CT: a phantom study. Eur Radiol 32:152–162. https://doi.org/10.1007/s00330-021-08152-w
26. Mergen V, Ghouse S, Sartoretti T et al (2023) Cardiac virtual noncontrast images for calcium quantification with photon-counting detector CT. Radiol Cardiothorac Imaging. https://doi.org/10.1148/ryct.220307
27. Ayoub C, Erthal F, Abdelsalam MA et al (2017) Prognostic value of segment involvement score compared to other measures of coronary atherosclerosis by computed tomography: a systematic review and meta-analysis. J Cardiovasc Comput Tomogr 11:258–267. https://doi.org/10.1016/j.jcct.2017.05.001
28. Tesche C, Plank F, De Cecco CN et al (2016) Prognostic implications of coronary CT angiography-derived quantitative markers for the prediction of major adverse cardiac events. J Cardiovasc Comput Tomogr 10:458–465. https://doi.org/10.1016/j.jcct.2016.08.003
29. Bittencourt MS, Hulten E, Ghoshhajra B et al (2014) Prognostic value of nonobstructive and obstructive coronary artery disease detected by coronary computed tomography angiography to identify cardiovascular events. Circ Cardiovasc Imaging 7:282–291. https://doi.org/10.1161/CIRCIMAGING.113.001047
30. Min JK, Shaw LJ, Devereux RB et al (2007) Prognostic value of multidetector coronary computed tomographic angiography for prediction of all-cause mortality. J Am Coll Cardiol 50:1161–1170. https://doi.org/10.1016/j.jacc.2007.03.067
31. Szilveszter B, Vattay B, Bossoussou M et al (2022) CAD-RADS may underestimate coronary plaque progression as detected by serial CT angiography. Eur Hear J Cardiovasc Imaging 23:1530–1539. https://doi.org/10.1093/ehjci/jeab215
32. Cury RC, Leipsic J, Abbara S et al (2022) CAD-RADS™ 2.0—2022 coronary artery disease-reporting and data system. J Cardiovasc Comput Tomogr 16:536–557. https://doi.org/10.1016/j.jcct.2022.07.002
33. de Araújo GP, Garcia-Garcia HM, Dores H et al (2013) Coronary computed tomography angiography-adapted Leaman score as a tool to noninvasively quantify total coronary atherosclerotic burden. Int J Cardiovasc Imaging 29:1575–1584. https://doi.org/10.1007/s10554-013-0232-8
34. Mushtaq S, Araujo de Gonçalves P, Garcia-Garcia HM et al (2015) Long-term prognostic effect of coronary atherosclerotic Burden. Circ Cardiovasc Imaging. https://doi.org/10.1161/CIRCIMAGING.114.002332
35. van Rosendael AR, Shaw LJ, Xie JX et al (2019) Superior risk stratification with coronary computed tomography angiography using a comprehensive atherosclerotic risk score. JACC Cardiovasc Imaging 12:1987–1997. https://doi.org/10.1016/j.jcmg.2018.10.024
36. van den Hoogen IJ, van Rosendael A, Lin F et al (2019) Coronary atherosclerosis scoring by the Leiden CCTA risk score for prediction of major adverse cardiac events: a propensity score-based analysis of diabetic and non-diabetic patients. J Am Coll Cardiol 73:1450. https://doi.org/10.1016/S0735-1097(19)32056-X
37. Kang D, Dey D, Slomka PJ et al (2015) Structured learning algorithm for detection of nonobstructive and obstructive coronary plaque lesions from computed tomography angiography. J Med Imaging 2:014003. https://doi.org/10.1117/1.JMI.2.1.014003
38. Sandstedt M, Henriksson L, Janzon M et al (2020) Evaluation of an AI-based, automatic coronary artery calcium scoring software. Eur Radiol 30:1671–1678. https://doi.org/10.1007/s00330-019-06489-x
39. Motoyama S, Ito H, Sarai M et al (2015) Plaque characterization by coronary computed tomography angiography and the likelihood of acute coronary events in mid-term follow-up. J Am Coll Cardiol 66:337–346. https://doi.org/10.1016/j.jacc.2015.05.069
40. Puchner SB, Liu T, Mayrhofer T et al (2014) High-risk plaque detected on coronary ct angiography predicts acute coronary syndromes independent of significant stenosis in acute chest pain. J Am Coll Cardiol 64:684–692. https://doi.org/10.1016/j.jacc.2014.05.039
41. Ferencik M, Mayrhofer T, Bittner DO et al (2018) Use of high-risk coronary atherosclerotic plaque detection for risk stratification of patients with stable chest pain. JAMA Cardiol 3:144. https://doi.org/10.1001/jamacardio.2017.4973
42. Achenbach S, Ropers D, Hoffmann U et al (2004) assessment of coronary remodeling in stenotic and nonstenotic coronary atherosclerotic lesions by multidetector spiral computed tomography. J Am Coll Cardiol 43:842–847. https://doi.org/10.1016/j.jacc.2003.09.053
43. Chang H-J, Lin FY, Lee S-E et al (2018) Coronary atherosclerotic precursors of acute coronary syndromes. J Am Coll Cardiol 71:2511–2522. https://doi.org/10.1016/j.jacc.2018.02.079
44. Oikonomou EK, West HW, Antoniades C (2019) Cardiac computed tomography. Arterioscler Thromb Vasc Biol 39:2207–2219. https://doi.org/10.1161/ATVBAHA.119.312899
45. Ferencik M, Schlett CL, Ghoshhajra BB et al (2012) A computed tomography-based coronary lesion score to predict acute coronary syndrome among patients with acute chest pain and significant coronary stenosis on coronary computed tomographic angiogram. Am J Cardiol 110:183–189. https://doi.org/10.1016/j.amjcard.2012.02.066
46. Benedek T, Gyöngyösi M, Benedek I (2013) Multislice computed tomographic coronary angiography for quantitative assessment of culprit lesions in acute coronary syndromes. Can J Cardiol 29:364–371. https://doi.org/10.1016/j.cjca.2012.11.004
47. Maurovich-Horvat P, Ferencik M, Voros S et al (2014) Comprehensive plaque assessment by coronary CT angiography. Nat Rev Cardiol 11:390–402. https://doi.org/10.1038/nrcardio.2014.60
48. Hadamitzky M, Taubert S, Deseive S et al (2013) Prognostic value of coronary computed tomography angiography during 5 years of follow-up in patients with suspected coronary artery disease. Eur Heart J 34:3277–3285. https://doi.org/10.1093/eurheartj/eht293
49. Hoffmann U, Ferencik M, Udelson JE et al (2017) Prognostic value of noninvasive cardiovascular testing in patients with stable chest pain. Circulation 135:2320–2332. https://doi.org/10.1161/CIRCULATIONAHA.116.024360
50. Motoyama S, Sarai M, Harigaya H et al (2009) Computed tomographic angiography characteristics of atherosclerotic

plaques subsequently resulting in acute coronary syndrome. J Am Coll Cardiol 54:49–57. https://doi.org/10.1016/j.jacc.2009.02.068
51. Otsuka K, Fukuda S, Tanaka A et al (2013) Napkin-ring sign on coronary ct angiography for the prediction of acute coronary syndrome. JACC Cardiovasc Imaging 6:448–457. https://doi.org/10.1016/j.jcmg.2012.09.016
52. Thomsen C, Abdulla J (2016) Characteristics of high-risk coronary plaques identified by computed tomographic angiography and associated prognosis: a systematic review and meta-analysis. Eur Hear J Cardiovasc Imaging 17:120–129. https://doi.org/10.1093/ehjci/jev325
53. von Knebel Doeberitz PL, De Cecco CN, Schoepf UJ et al (2019) Coronary CT angiography–derived plaque quantification with artificial intelligence CT fractional flow reserve for the identification of lesion-specific ischemia. Eur Radiol 29:2378–2387. https://doi.org/10.1007/s00330-018-5834-z
54. Pérez de Isla L, Alonso R, Gómez de Diego JJ et al (2021) Coronary plaque burden, plaque characterization and their prognostic implications in familial hypercholesterolemia: a computed tomographic angiography study. Atherosclerosis 317:52–58. https://doi.org/10.1016/j.atherosclerosis.2020.11.012
55. Kolossváry M, Karády J, Szilveszter B et al (2017) Radiomic features are superior to conventional quantitative computed tomographic metrics to identify coronary plaques with napkin-ring sign. Circ Cardiovasc Imaging. https://doi.org/10.1161/CIRCIMAGING.117.006843
56. Kolossváry M, Park J, Bang J-I et al (2019) Identification of invasive and radionuclide imaging markers of coronary plaque vulnerability using radiomic analysis of coronary computed tomography angiography. Eur Hear J Cardiovasc Imaging 20:1250–1258. https://doi.org/10.1093/ehjci/jez033
57. Moss AJ, Williams MC, Newby DE, Nicol ED (2017) The updated NICE guidelines: cardiac CT as the first-line test for coronary artery disease. Curr Cardiovasc Imaging Rep 10:15
58. Lu MT, Ferencik M, Roberts RS et al (2017) Noninvasive FFR derived from coronary CT angiography: management and outcomes in the PROMISE trial. JACC Cardiovasc Imaging 10:1350–1358. https://doi.org/10.1016/j.jcmg.2016.11.024
59. Rajiah P, Cummings KW, Williamson E, Young PM (2022) CT fractional flow reserve: a practical guide to application, interpretation, and problem solving. Radiographics 42:340–358. https://doi.org/10.1148/rg.210097
60. Taylor CA, Fonte TA, Min JK (2013) Computational fluid dynamics applied to cardiac computed tomography for noninvasive quantification of fractional flow reserve: Scientific basis. J Am Coll Cardiol 61:2233–2241. https://doi.org/10.1016/j.jacc.2012.11.083
61. Baumann S, Hirt M, Rott C et al (2020) Comparison of machine learning computed tomography-based fractional flow reserve and coronary CT angiography-derived plaque characteristics with invasive resting full-cycle ratio. J Clin Med 9:714. https://doi.org/10.3390/jcm9030714
62. Giannopoulos AA, Keller L, Sepulcri D et al (2023) High-speed onsite deep-learning based FFR-CT algorithm: evaluation using invasive angiography as reference standard. Am J Roentgenol. https://doi.org/10.2214/AJR.23.29156
63. Zimmermann FM, Mast TP, Johnson NP et al (2021) Deep learning for prediction of fractional flow reserve from resting coronary pressure curves. EuroIntervention 17:51–58. https://doi.org/10.4244/EIJ-D-20-00648
64. Tesche C, Gray HN (2020) Machine learning and deep neural networks applications in coronary flow assessment. J Thorac Imaging 35:S66–S71. https://doi.org/10.1097/RTI.0000000000000483
65. Coenen A, Kim Y-H, Kruk M et al (2018) Diagnostic accuracy of a machine-learning approach to coronary computed tomographic angiography-based fractional flow reserve. Circ Cardiovasc Imaging. https://doi.org/10.1161/CIRCIMAGING.117.007217
66. Yang J, Shan D, Dong M et al (2020) The effect of on-site CT-derived fractional flow reserve on the management of decision making for patients with stable chest pain (TARGET trial): objective, rationale, and design. Trials 21:728. https://doi.org/10.1186/s13063-020-04649-9
67. Koo BK, Erglis A, Doh JH et al (2011) Diagnosis of ischemia-causing coronary stenoses by noninvasive fractional flow reserve computed from coronary computed tomographic angiograms: results from the prospective multicenter DISCOVER-FLOW (Diagnosis of Ischemia-Causing Stenoses Obtained Via Noni. J Am Coll Cardiol 58:1989–1997. https://doi.org/10.1016/j.jacc.2011.06.066
68. Douglas PS, De Bruyne B, Pontone G et al (2016) 1-Year outcomes of FFRCT-guided care in patients with suspected coronary disease: the platform study. J Am Coll Cardiol 68:435–445. https://doi.org/10.1016/j.jacc.2016.05.057
69. Hlatky MA, Saxena A, Koo B-K et al (2013) Projected costs and consequences of computed tomography-determined fractional flow reserve. Clin Cardiol 36:743–748. https://doi.org/10.1002/clc.22205
70. Fischer AM, van Assen M, Schoepf UJ et al (2021) Non-invasive fractional flow reserve (FFRCT) in the evaluation of acute chest pain—concepts and first experiences. Eur J Radiol 138:109633. https://doi.org/10.1016/j.ejrad.2021.109633
71. Gulati M, Levy PD, Mukherjee D et al (2021) 2021 AHA/ACC/ASE/CHEST/SAEM/SCCT/SCMR guideline for the evaluation and diagnosis of chest pain: A report of the American college of cardiology/American heart association joint committee on clinical practice guidelines. Circulation. https://doi.org/10.1161/CIR.0000000000001029
72. Nørgaard BL, Leipsic J, Gaur S et al (2014) Diagnostic performance of noninvasive fractional flow reserve derived from coronary computed tomography angiography in suspected coronary artery disease. J Am Coll Cardiol 63:1145–1155. https://doi.org/10.1016/j.jacc.2013.11.043
73. Tesche C, De Cecco CN, Albrecht MH et al (2017) Coronary CT angiography–derived fractional flow reserve. Radiology 285:17–33. https://doi.org/10.1148/radiol.2017162641
74. Pontone G, Weir-McCall JR, Baggiano A et al (2019) Determinants of rejection rate for coronary CT angiography fractional flow reserve analysis. Radiology 292:597–605. https://doi.org/10.1148/radiol.2019182673
75. Feng Y, Xu Z, Zhang L et al (2022) Machine-learning-derived radiomics signature of pericoronary tissue in coronary CT angiography associates with functional ischemia. Front Physiol. https://doi.org/10.3389/fphys.2022.980996
76. Oikonomou EK, Williams MC, Kotanidis CP et al (2019) A novel machine learning-derived radiotranscriptomic signature of perivascular fat improves cardiac risk prediction using coronary CT angiography. Eur Heart J 40:3529–3543. https://doi.org/10.1093/eurheartj/ehz592
77. Antonopoulos AS, Sanna F, Sabharwal N et al (2017) Detecting human coronary inflammation by imaging perivascular fat. Sci Transl Med. https://doi.org/10.1126/scitranslmed.aal2658
78. van der Bijl P, Kuneman JH, Bax JJ (2022) Pericoronary adipose tissue attenuation: diagnostic and prognostic implications. Eur Hear J Cardiovasc Imaging 23:e537–e538. https://doi.org/10.1093/ehjci/jeac175
79. Sagris M, Antonopoulos AS, Simantiris S et al (2022) Pericoronary fat attenuation index—a new imaging biomarker and its diagnostic and prognostic utility: a systematic review and

meta-analysis. Eur Hear J - Cardiovasc Imaging 23:e526–e536. https://doi.org/10.1093/ehjci/jeac174
80. Oikonomou EK, Marwan M, Desai MY et al (2018) Non-invasive detection of coronary inflammation using computed tomography and prediction of residual cardiovascular risk (the CRISP CT study): a post-hoc analysis of prospective outcome data. Lancet 392:929–939. https://doi.org/10.1016/S0140-6736(18)31114-0
81. Lin A, Kolossváry M, Yuvaraj J et al (2020) Myocardial infarction associates with a distinct pericoronary adipose tissue radiomic phenotype. JACC Cardiovasc Imaging 13:2371–2383. https://doi.org/10.1016/j.jcmg.2020.06.033
82. Varga-Szemes A, Meinel FG, De Cecco CN et al (2015) CT myocardial perfusion imaging. Am J Roentgenol 204:487–497. https://doi.org/10.2214/AJR.14.13546
83. Pontone G, Baggiano A, Andreini D et al (2019) Dynamic stress computed tomography perfusion with a whole-heart coverage scanner in addition to coronary computed tomography angiography and fractional flow reserve computed tomography derived. JACC Cardiovasc Imaging 12:2460–2471. https://doi.org/10.1016/j.jcmg.2019.02.015
84. Bamberg F, Becker A, Schwarz F et al (2011) Detection of hemodynamically significant coronary artery stenosis: incremental diagnostic value of dynamic CT-based myocardial perfusion imaging. Radiology 260:689–698. https://doi.org/10.1148/radiol.11110638
85. Rossi A, Dharampal A, Wragg A et al (2014) Diagnostic performance of hyperaemic myocardial blood flow index obtained by dynamic computed tomography: does it predict functionally significant coronary lesions? Eur Hear J Cardiovasc Imaging 15:85–94. https://doi.org/10.1093/ehjci/jet133
86. Coenen A, Rossi A, Lubbers MM et al (2017) Integrating CT myocardial perfusion and CT-FFR in the work-up of coronary artery disease. JACC Cardiovasc Imaging 10:760–770. https://doi.org/10.1016/j.jcmg.2016.09.028
87. Tanabe Y, Kido T, Uetani T et al (2016) Differentiation of myocardial ischemia and infarction assessed by dynamic computed tomography perfusion imaging and comparison with cardiac magnetic resonance and single-photon emission computed tomography. Eur Radiol 26:3790–3801. https://doi.org/10.1007/s00330-016-4238-1
88. Alessio AM, Bindschadler M, Busey JM et al (2019) Accuracy of myocardial blood flow estimation from dynamic contrast-enhanced cardiac CT compared With PET. Circ Cardiovasc Imaging. https://doi.org/10.1161/CIRCIMAGING.118.008323
89. Lu M, Wang S, Sirajuddin A et al (2018) Dynamic stress computed tomography myocardial perfusion for detecting myocardial ischemia: a systematic review and meta-analysis. Int J Cardiol 258:325–331. https://doi.org/10.1016/j.ijcard.2018.01.095
90. Lubbers M, Coenen A, Kofflard M et al (2018) Comprehensive cardiac CT with myocardial perfusion imaging versus functional testing in suspected coronary artery disease: the multicenter, randomized CRESCENT-II trial. JACC Cardiovasc Imaging 11:1625–1636. https://doi.org/10.1016/j.jcmg.2017.10.010
91. Nakamura S, Kitagawa K, Goto Y et al (2019) Incremental prognostic value of myocardial blood flow quantified with stress dynamic computed tomography perfusion imaging. JACC Cardiovasc Imaging 12:1379–1387. https://doi.org/10.1016/j.jcmg.2018.05.021
92. Yu M, Chen X, Dai X et al (2019) The value of low-dose dynamic myocardial perfusion CT for accurate evaluation of microvascular obstruction in patients with acute myocardial infarction. Am J Roentgenol 213:798–806. https://doi.org/10.2214/AJR.19.21305
93. Galea N, Dacquino GM, Ammendola RM et al (2019) Microvascular obstruction extent predicts major adverse cardiovascular events in patients with acute myocardial infarction and preserved ejection fraction. Eur Radiol 29:2369–2377. https://doi.org/10.1007/s00330-018-5895-z
94. Vliegenthart R, Pelgrim GJ, Ebersberger U et al (2012) Dual-energy CT of the heart. Am J Roentgenol 199:S54–S63. https://doi.org/10.2214/AJR.12.9208
95. Nakahara T, Toyama T, Jinzaki M et al (2018) Quantitative analysis of iodine image of dual-energy computed tomography at rest. J Thorac Imaging 33:97–104. https://doi.org/10.1097/RTI.0000000000000284
96. Dell'Aversana S, Ascione R, De Giorgi M et al (2022) Dual-energy CT of the heart: a review. J Imaging 8:236. https://doi.org/10.3390/jimaging8090236
97. Kumar V, Harfi TT, He X et al (2019) Estimation of myocardial fibrosis in humans with dual energy CT. J Cardiovasc Comput Tomogr 13:315–318. https://doi.org/10.1016/j.jcct.2018.12.004
98. van Assen M, Vonder M, Pelgrim GJ et al (2020) Computed tomography for myocardial characterization in ischemic heart disease: a state-of-the-art review. Eur Radiol Exp 4:36. https://doi.org/10.1186/s41747-020-00158-1
99. Palmisano A, Vignale D, Benedetti G et al (2020) Late iodine enhancement cardiac computed tomography for detection of myocardial scars: impact of experience in the clinical practice. Radiol Med 125:128–136. https://doi.org/10.1007/s11547-019-01108-7
100. Pattanayak P, Bleumke DA (2015) Tissue characterization of the myocardium. Radiol Clin North Am 53:413–423. https://doi.org/10.1016/j.rcl.2014.11.005
101. Tanabe Y, Kido T, Kurata A et al (2017) Impact of knowledge-based iterative model reconstruction on myocardial late iodine enhancement in computed tomography and comparison with cardiac magnetic resonance. Int J Cardiovasc Imaging 33:1609–1618. https://doi.org/10.1007/s10554-017-1137-8
102. Wichmann JL, Bauer RW, Doss M et al (2013) Diagnostic accuracy of late iodine-enhancement dual-energy computed tomography for the detection of chronic myocardial infarction compared with late gadolinium-enhancement 3-t magnetic resonance imaging. Invest Radiol 48:851–856. https://doi.org/10.1097/RLI.0b013e31829d91a8
103. Matsuda T, Kido T, Itoh T et al (2015) Diagnostic accuracy of late iodine enhancement on cardiac computed tomography with a denoise filter for the evaluation of myocardial infarction. Int J Cardiovasc Imaging 31:177–185. https://doi.org/10.1007/s10554-015-0716-9
104. Bouleti C, Baudry G, Iung B et al (2017) Usefulness of late iodine enhancement on spectral CT in acute myocarditis. JACC Cardiovasc Imaging 10:826–827. https://doi.org/10.1016/j.jcmg.2016.09.013
105. Ohta Y, Kitao S, Yunaga H et al (2018) Myocardial delayed enhancement CT for the evaluation of heart failure: comparison to MRI. Radiology 288:682–691. https://doi.org/10.1148/radiol.2018172523
106. Palmisano A, Vignale D, Tadic M et al (2022) Myocardial late contrast enhancement CT in troponin-positive acute chest pain syndrome. Radiology 302:545–553. https://doi.org/10.1148/radiol.211288
107. Esposito A, Palmisano A, Antunes S et al (2016) Cardiac CT with delayed enhancement in the characterization of ventricular tachycardia structural substrate. JACC Cardiovasc Imaging 9:822–832. https://doi.org/10.1016/j.jcmg.2015.10.024
108. Scully PR, Bastarrika G, Moon JC, Treibel TA (2018) Myocardial extracellular volume quantification by cardiovascular magnetic resonance and computed tomography. Curr Cardiol Rep 20:15. https://doi.org/10.1007/s11886-018-0961-3
109. Bandula S, White SK, Flett AS et al (2013) Measurement of myocardial extracellular volume fraction by using equilibrium contrast-enhanced CT: validation against histologic findings.

Radiology 269:396–403. https://doi.org/10.1148/radiology.13130130
110. Abadia AF, van Assen M, Martin SS et al (2020) Myocardial extracellular volume fraction to differentiate healthy from cardiomyopathic myocardium using dual-source dual-energy CT. J Cardiovasc Comput Tomogr 14:162–167. https://doi.org/10.1016/j.jcct.2019.09.008
111. Hayashi H, Oda S, Emoto T et al (2022) Myocardial extracellular volume quantification by cardiac CT in pulmonary hypertension: comparison with cardiac MRI. Eur J Radiol 153:110386. https://doi.org/10.1016/j.ejrad.2022.110386
112. Aquino GJ, O'Doherty J, Schoepf UJ et al (2023) Myocardial characterization with extracellular volume mapping with a first-generation photon-counting detector CT with MRI reference. Radiology 307:e222030. https://doi.org/10.1148/radiol.222030
113. Mergen V, Sartoretti T, Klotz E et al (2022) Extracellular volume quantification with cardiac late enhancement scanning using dual-source photon-counting detector CT. Invest Radiol 57:406–411. https://doi.org/10.1097/RLI.0000000000000851
114. Lee H-J, Im DJ, Youn J-C et al (2016) Myocardial extracellular volume fraction with dual-energy equilibrium contrast-enhanced cardiac CT in nonischemic cardiomyopathy: a prospective comparison with cardiac MR imaging. Radiology 280:49–57. https://doi.org/10.1148/radiol.2016151289
115. Ohta Y, Kishimoto J, Kitao S et al (2020) Investigation of myocardial extracellular volume fraction in heart failure patients using iodine map with rapid-kV switching dual-energy CT: segmental comparison with MRI T1 mapping. J Cardiovasc Comput Tomogr 14:349–355. https://doi.org/10.1016/j.jcct.2019.12.032
116. Tamarappoo B, Han D, Tyler J et al (2020) Prognostic value of computed tomography-derived extracellular volume in TAVR patients with low-flow low-gradient aortic stenosis. JACC Cardiovasc Imaging 13:2591–2601. https://doi.org/10.1016/j.jcmg.2020.07.045
117. Nacif MS, Kawel N, Lee JJ et al (2012) Interstitial myocardial fibrosis assessed as extracellular volume fraction with low-radiation-dose cardiac CT. Radiology 264:876–883. https://doi.org/10.1148/radiol.12112458
118. Hamdy A, Kitagawa K, Goto Y et al (2019) Comparison of the different imaging time points in delayed phase cardiac CT for myocardial scar assessment and extracellular volume fraction estimation in patients with old myocardial infarction. Int J Cardiovasc Imaging 35:917–926. https://doi.org/10.1007/s10554-018-1513-z
119. Qi R-X, Jiang J-S, Shao J et al (2022) Measurement of myocardial extracellular volume fraction in patients with heart failure with preserved ejection fraction using dual-energy computed tomography. Eur Radiol 32:4253–4263. https://doi.org/10.1007/s00330-021-08514-4
120. Yashima S, Takaoka H, Iwahana T et al (2023) Evaluation of extracellular volume by computed tomography is useful for prediction of prognosis in dilated cardiomyopathy. Heart Vessels 38:185–194. https://doi.org/10.1007/s00380-022-02154-4
121. Gama F, Rosmini S, Bandula S et al (2022) Extracellular volume fraction by computed tomography predicts long-term prognosis among patients with cardiac amyloidosis. JACC Cardiovasc Imaging 15:2082–2094. https://doi.org/10.1016/j.jcmg.2022.08.006
122. Ishiyama M, Kurita T, Takafuji M et al (2023) The cardiac computed tomography-derived extracellular volume fraction predicts patient outcomes and left ventricular mass reductions after transcatheter aortic valve implantation for aortic stenosis. J Cardiol 81:476–484. https://doi.org/10.1016/j.jjcc.2022.12.002
123. Han D, Tamarappoo B, Klein E et al (2021) Computed tomography angiography-derived extracellular volume fraction predicts early recovery of left ventricular systolic function after transcatheter aortic valve replacement. Eur Hear J Cardiovasc Imaging 22:179–185. https://doi.org/10.1093/ehjci/jeaa310
124. Gaborit B, Sengenes C, Ancel P, et al (2017) Role of Epicardial Adipose Tissue in Health and Disease: A Matter of Fat? In: Comprehensive Physiology. Wiley, pp 1051–1082
125. Mancio J, Azevedo D, Saraiva F et al (2018) Epicardial adipose tissue volume assessed by computed tomography and coronary artery disease: a systematic review and meta-analysis. Eur Hear J Cardiovasc Imaging 19:490–497. https://doi.org/10.1093/ehjci/jex314
126. Cannavale G, Francone M, Galea N et al (2018) Fatty images of the heart: spectrum of normal and pathological findings by computed tomography and cardiac magnetic resonance imaging. Biomed Res Int 2018:1–13. https://doi.org/10.1155/2018/5610347
127. Mahabadi AA, Berg MH, Lehmann N et al (2013) Association of epicardial fat with cardiovascular risk factors and incident myocardial infarction in the general population. J Am Coll Cardiol 61:1388–1395. https://doi.org/10.1016/j.jacc.2012.11.062
128. Antonopoulos AS, Antoniades C (2017) The role of epicardial adipose tissue in cardiac biology: classic concepts and emerging roles. J Physiol 595:3907–3917. https://doi.org/10.1113/JP273049
129. Zhu W, Zhang H, Guo L, Hong K (2016) Relationship between epicardial adipose tissue volume and atrial fibrillation. Herz 41:421–427. https://doi.org/10.1007/s00059-015-4387-z
130. Yorgun H, Canpolat U, Aytemir K et al (2015) Association of epicardial and peri-atrial adiposity with the presence and severity of non-valvular atrial fibrillation. Int J Cardiovasc Imaging 31:649–657. https://doi.org/10.1007/s10554-014-0579-5
131. Venkateshvaran A, Faxen UL, Hage C et al (2022) Association of epicardial adipose tissue with proteomics, coronary flow reserve, cardiac structure and function, and quality of life in heart failure with preserved ejection fraction: insights from the <scp>PROMIS-HFpEF</scp> study. Eur J Heart Fail 24:2251–2260. https://doi.org/10.1002/ejhf.2709
132. La Grutta L, Toia P, Farruggia A et al (2016) Quantification of epicardial adipose tissue in coronary calcium score and CT coronary angiography image data sets: comparison of attenuation values, thickness and volumes. Br J Radiol 89:20150773. https://doi.org/10.1259/bjr.20150773
133. Raggi P, Gadiyaram V, Zhang C et al (2019) Statins reduce epicardial adipose tissue attenuation independent of lipid lowering: a potential pleiotropic effect. J Am Heart Assoc. https://doi.org/10.1161/JAHA.119.013104
134. Franssens BT, Nathoe HM, Visseren FLJ et al (2017) Relation of epicardial adipose tissue radiodensity to coronary artery calcium on cardiac computed tomography in patients at high risk for cardiovascular disease. Am J Cardiol 119:1359–1365. https://doi.org/10.1016/j.amjcard.2017.01.031
135. Goeller M, Achenbach S, Marwan M et al (2018) Epicardial adipose tissue density and volume are related to subclinical atherosclerosis, inflammation and major adverse cardiac events in asymptomatic subjects. J Cardiovasc Comput Tomogr 12:67–73. https://doi.org/10.1016/j.jcct.2017.11.007
136. Gaibazzi N, Martini C, Botti A et al (2019) Coronary inflammation by computed tomography pericoronary fat attenuation in MINOCA and Tako-Tsubo syndrome. J Am Heart Assoc. https://doi.org/10.1161/JAHA.119.013235
137. Nichols JH, Samy B, Nasir K et al (2008) Volumetric measurement of pericardial adipose tissue from contrast-enhanced coronary computed tomography angiography: a reproducibility study. J Cardiovasc Comput Tomogr 2:288–295. https://doi.org/10.1016/j.jcct.2008.08.008

138. Barbosa JG, Figueiredo B, Bettencourt N, Tavares JMRS (2011) toward automatic quantification of the epicardial fat in non-contrasted CT images. Comput Methods Biomech Biomed Eng 14:905–914. https://doi.org/10.1080/10255842.2010.499871
139. Rebelo AF, Ferreira AM, Fonseca JM (2022) Automatic epicardial fat segmentation and volume quantification on non-contrast cardiac Computed Tomography. Comput Methods Programs Biomed Updat 2:100079. https://doi.org/10.1016/j.cmpbup.2022.100079
140. Ding X, Terzopoulos D, Diaz-Zamudio M et al (2015) Automated pericardium delineation and epicardial fat volume quantification from noncontrast CT. Med Phys 42:5015–5026. https://doi.org/10.1118/1.4927375
141. Commandeur F, Goeller M, Betancur J et al (2018) Deep learning for quantification of epicardial and thoracic adipose tissue from non-contrast CT. IEEE Trans Med Imaging 37:1835–1846. https://doi.org/10.1109/TMI.2018.2804799
142. Commandeur F, Goeller M, Razipour A et al (2019) Fully automated CT quantification of epicardial adipose tissue by deep learning: a multicenter study. Radiol Artif Intell 1:e190045. https://doi.org/10.1148/ryai.2019190045
143. Gillies RJ, Kinahan PE, Hricak H (2016) Radiomics: images are more than pictures, they are data. Radiology 278:563–577. https://doi.org/10.1148/radiol.2015151169
144. Hu W, Wu X, Dong D et al (2020) Novel radiomics features from CCTA images for the functional evaluation of significant ischemic lesions based on the coronary fractional flow reserve score. Int J Cardiovasc Imaging 36:2039–2050. https://doi.org/10.1007/s10554-020-01896-4
145. Kolossváry M, Karády J, Kikuchi Y et al (2019) Radiomics versus visual and histogram-based assessment to identify atheromatous lesions at coronary CT angiography: an ex vivo study. Radiology 293:89–96. https://doi.org/10.1148/radiol.2019190407
146. Li L, Hu X, Tao X et al (2021) Radiomic features of plaques derived from coronary CT angiography to identify hemodynamically significant coronary stenosis, using invasive FFR as the reference standard. Eur J Radiol 140:109769. https://doi.org/10.1016/j.ejrad.2021.109769
147. Mannil M, von Spiczak J, Manka R, Alkadhi H (2018) Texture analysis and machine learning for detecting myocardial infarction in noncontrast low-dose computed tomography. Invest Radiol 53:338–343. https://doi.org/10.1097/RLI.0000000000000448
148. Shu Z-Y, Cui S-J, Zhang Y-Q et al (2022) Predicting chronic myocardial ischemia using CCTA-based radiomics machine learning nomogram. J Nucl Cardiol 29:262–274. https://doi.org/10.1007/s12350-020-02204-2
149. Qian W, Jiang Y, Liu X et al (2021) Distinguishing cardiac myxomas from cardiac thrombi by a radiomics signature based on cardiovascular contrast-enhanced computed tomography images. BMC Cardiovasc Disord 21:152. https://doi.org/10.1186/s12872-021-01961-3
150. Shang J, Guo Y, Ma Y, Hou Y (2022) Cardiac computed tomography radiomics: a narrative review of current status and future directions. Quant Imaging Med Surg 12:3436–3453. https://doi.org/10.21037/qims-21-1022
151. Motwani M, Dey D, Berman DS et al (2016) Machine learning for prediction of all-cause mortality in patients with suspected coronary artery disease: a 5-year multicentre prospective registry analysis. Eur Heart J ehw. https://doi.org/10.1093/eurheartj/ehw188
152. Cundari G, Galea N, Mergen V et al (2023) Myocardial extracellular volume quantification with computed tomography-current status and future outlook. Insights Imaging 14:156. https://doi.org/10.1186/s13244-023-01506-6